Numerical Simulations of Nonequilibrium Flows over Rounded Models at Reentry Speeds

Chih-Yung Wen*

Department of Mechanical Engineering, The Hong Kong Polytechnic University, Kowloon, Hong Kong

Heriberto Saldívar Massimi†

Department of Aeronautics and Astronautics, National Cheng Kung University, Tainan, Taiwan 70101

Yen-Sen Chen‡

National Space Organization, Hsinchu Science Park, Hsinchu, Taiwan 30078

Shen-Min Liang§

Department of Computer Application Engineering, Far East University, Taiwan 744

Yevgeniy A. Bondar¶ and Mikhail S. Ivanov ‖

Khristianovich Institute of Theoretical and Applied Mechanics SB RAS, Novosibirsk, Russia 630090

The present work focuses on the problem of aerothermodynamics of space vehicles with rounded edges on the hypersonic segment of the flight trajectory. Firstly, the in-house Navier-Stokes solver, UNIC-UNS code, with the slip boundary condition is used to simulate the flows around a spherical-nosed cylinder at different Knudsen numbers and Mach numbers, and compared with DSMC computations for validation. The Navier-Stokes simulations are in good agreement with that of DSMC. The hypersonic flows over the European eXPErimental Re-entry Test-bed (EXPERT) model are then simulated for a wide range of flow regimes, which correspond to the expected descent trajectory with allowance for rarefaction and thermochemical nonequilibrium. Three dimensional CFD analyses are presented for the complete geometry of the capsules considering the air dissociation and its effects on the flow structure and on the force and thermal loads for the hypersonic segment of the flight as a precursor to the future studies and to provide the scientific community with quality data that can be used to improve tools for the design of hypersonic vehicles.

Nomenclature

a	Speed of sound
$ALPS$	Advanced Large-scale Parallel Supercluster
AoA	Angle of attack

*Professor, Department of Mechanical Engineering, The Hong Kong Polytechnic University, Kowloon, Hong Kong, and AIAA Associate Fellow.

†Master student, Department of Aeronautics and Astronautics, National Cheng Kung University, No.1 University Road, Tainan, Taiwan 701, and AIAA Member.

‡Senior Research Fellow and Suborbital Rocket Experiment Program Director, National Space Organization, 8F, 9, Prosperity 1st Rd., Hsinchu Science Park, Hsinchu, Taiwan 30078, and AIAA Associate Fellow.

§Professor, Department of Computer Application Engineering, Far East University, No.49, Chung Hua Rd., Hsin-Shih. Tainan County 744, Taiwan, AIAA Associate Fellow

¶Senior Research Scientist, PhD. Computational Aerodynamics Laboratory, Khristianovich Institute of Theoretical and Applied Mechanics Sb RAS, Institutskaya str. 4/1, Novosibirsk 6300090, Russia.

‖Professor, Head of computational Aerodynamics Laboratory, Khristianovich Institute of Theoretical and Applied Mechanics SB RAS, Institutskaya str. 4/1, Novosibirsk 630090, Russia, and AIAA Fellow

C	Pre-exponential factor in reaction rate coefficient, $\frac{cm^3}{moles}$
C_f	Skin friction coefficient
CFD	Computational fluid dynamics
C_h	Stanton number
C_p	Pressure coefficient
D	Diameter
$DSMC$	Direct simulation Monte Carlo
E	Reaction Energy
$EXPERT$	European eXPErimental Re-entry Test-bed
$ICBM$	Intercontinental ballistic missile
k	Boltzmann constant
Kn	Knudsen number
Ma	Mach number
MPI	Message passing interface
NS	Navier Stokes
p	Pressure
p_∞	Free stream pressure
q	Convection heat transfer coefficient
R	Gas constant
Re	Reynolds number
RCB	Recursive coordinate bisection
RGB	Recursive graph bisection
$SIMPLE$	Semi-Implicit Method for Pressure-Linked Equations
T	Temperature
T_v	Vibrational-electron translational-electronic temperature
T_w	Wall temperature
T_x	Controlling temperature
V	Velocity
V_∞	Free stream velocity
$\sqrt{TT_v}$	Geometrically averaged temperature
γ	Specific heat ratio
$\triangle$	Standoff distance
ρ_s	Density on the stagnation streamline and just behind the shock
ρ_∞	Free stream density
τ_w	Shear stress

I. Introduction

The development of promising space vehicles requires detailed knowledge of their aerothermodynamics at high flight speeds and altitudes. For this reason, it is necessary to study phenomena associated with rarefaction and thermochemical nonequilibrium of the gas in a hypersonic flow. Typical parameters (Mach numbers, Ma, and Knudsen numbers, Kn, of the flow around the space vehicle at high altitudes are beyond the capabilities of ground-based facilities; therefore, numerical methods of rarefied gas dynamics have become practically the only possible tool for studying these phenomena. In studying aerothermodynamics of space vehicles on the hypersonic segment of the flight trajectory with different flight regimes being formed, it is necessary to use a combination of the Direct Simulation Monte Carlo (DSMC) method for the transitional flow regime and Navier-Stokes (NS) equations for the continuum flow regime. Note that it is only such combined numerical investigations with the use of both kinetic and continuum approaches that provide detailed information on the flow structure and also on the force and thermal loads for the hypersonic segments of the flight trajectory. The first stage of the work focuses on flows around a spherical-nosed cylinder at $Ma = 5$, 10 and 20 and $Kn = 0.06$ and 0.5. The second stage is to simulate the flows over the European eXPErimental Re-entry Test-bed (EXPERT) model [1], where the flow regimes, correspond to those of the expected descent trajectory, 90 km down to 60 km. The EXPERT reentry vehicle was developed to provide the scientific community with quality data that can be used to improve tools for the design

of hypersonic vehicles. EXPERT is classified as a flight test-bed to pursue the investigation of specific hypersonic phenomena. EXPERT will fly in a suborbital ballistic trajectory from the Pacific Ocean to a landing site located on the peninsula of Kamchatka. EXPERT will be launched onboard a Russian converted ICBM, Volna, from a submarine. The re-entry speed selected at the entry gate of 100km altitude is 5 km/s. After the re-entry phase, EXPERT will be slowed down using a 3-stage parachute system that will allow a safe landing speed lower than 10m/s.

II. Geometry and Computational Domain

A. Spherical-Nosed Cylinder

In order to validate the in-house NS solver, UNIC-UNS [2] code with the slip boundary condition, perfect gas (Argon) and Non-reacting Nitrogen flows over a spherical-nosed cylinder are simulated and compared with DSMC[3] computations. The schematic diagram of the model with the radius set as the reference length equal to 1 unit used to study the characteristic flow field around it is shown in Fig. 1, including boundary conditions.

B. EXPERT

The EXPERT configuration (Fig. 2) is a blunted pyramidal shape featuring four flaps. The nose is made in the form of an ellipse with an eccentricity of 0.9165. The local radius of the nose part is 0.6 m. The ellipse-cone junction is described by a clothoid. The conical body has a cone angle of 12.5°. The cone is truncated by planes at an angle of 8.35°to the axis of symmetry. Four control flaps are deflected by 20°. To calculate the Reynolds numbers (Re) and the Knudsen numbers (Kn), the nose diameter, D = 1.2 m and the nose radius, D/2 were adopted as the reference lengths, respectively. The computational domain applied to the EXPERT capsule simulations is shown in Fig. 3, along with the corresponding boundary conditions. As seen, the domain is bounded between the supersonic inlet and the outlet. The model is positioned with an angle of attack (AoA) of 5.5°. A hybrid mesh of 9,326,336 cells composes the computational domain.

The capsule's Knudsen and Reynolds numbers vary according to the altitudes (see Fig. 4). During the descent trajectory, the free stream Knudsen number varies from free-molecular flow to continuum flow and the Reynolds number varies from laminar flow to turbulent flow.

III. Numerical Method and Test Cases

A. Numerical Method

The in-house UNIC-UNS code [2] is used for Navier-Stokes computations of thermally and chemically nonequilibrium airflow. The SMILE software system [3] is employed for DSMC computations to validate the UNIC-UNS code. The UNIC-UNS code, which is developed for predicting all speed flows that employs solution methods based on modified pressure-velocity coupling algorithms related to the SIMPLE-type, is used to study the flow around the vehicle. The primary variables in the code are the Cartesian velocity components, pressure, total enthalpy, turbulence kinetic energy, turbulence dissipation and mass fractions of chemical species. Finite-rate chemistry model with 11 species and 31 reactions and extended k-epsilon turbulence model with compressibility correction are used in the computation. The pressure correction equation is formulated using the perturbed equation of state, momentum and continuity equations. Because satisfaction of the continuity equation is of crucial importance to guarantee the overall convergence, most of the computing time in fluid flow calculation is spent on solving the pressure-correction equation by which the continuity-satisfying flow field is enforced. Therefore the preconditioned Bi-CGSTAB and GMRES matrix solvers are used to efficiently solve, respectively, the transport equations and the pressure-correction equation. A dual-time sub-iteration method is used in UNIC-UNS for time accurate time-marching computations.

The code is parallelized with Message Passing Interface (MPI). In performing parallel computation, domain decomposition method is currently used in the code. Both recursive coordinate bisection (RCB) method and recursive graph bisection (RGB) method in a publicly available package developed at University of Minnesota, METIS, are employed for efficient decomposition.

The ALPS cluster, a system that offers an aggregate performance of over 177 TFLOPS, uses the AMDR Opteron 6100 processors, and has a total of 8 compute clusters, 1 large memory cluster, and over 25,600

compute cores is used for the numerical simulations. The cluster is supported by the National Center for High-performance Computing in Hsinchu, R.O.C. Taiwan.

B. Test cases

For the spherical-nosed cylinder, the simulations are performed for the validation of UNIC-UNS code. The free-stream conditions for all the test cases are shown in Table 1. Both Argon and Nitrogen are adopted as the test gas. The gas parameters of Argon and Nitrogen are shown in Table 2 and Table 3, respectively. For the EXPERT model, the simulations include a wide range of flow regimes, which correspond to the expected descent trajectory from 90km down to 60km of altitude with allowance for rarefaction and thermochemical nonequilibrium. The test parameters are listed in Table 4.

C. Park's Two-Temperature Model

It has been pointed out that the one-temperature description to the flow leads to a substantial overestimation of the rate of equilibration when compared with the experimental data. The in-house UNIC-UNS code uses a two temperature chemical-kinetic model developed by Park [4]. The model uses one temperature T to characterize the translational energies of both atoms and molecules and the rotational energy of the molecules, and another temperature T_v. to characterize the vibrational energy of the molecules. The reaction rates are calculated with the geometrical-averaged temperature, $T_x = \sqrt{T\ Tv}$. The reaction rate parameters are defined by the forward-rate coefficient expression (Eq. (1)) and are presented in Table 5.

$$k_f \ = \ C\ T_x^n exp\left(\frac{-E}{k\ T_x}\right) \tag{1}$$

In Eq. (1), k_f is the forward reaction rate, C the reaction rate constant, n the temperature exponent on reaction-rate coefficient, k the Boltzmann constant, and E the Reaction Energy.

D. Slip Boundary Conditions

The slip boundary conditions [5] for the wall slip velocity,u_w, is as follows:

$$u_w \approx \left(\frac{2}{f}-1\right) l \left(\frac{du}{dy}\right)_w \ , where\ l = \frac{3}{2}\left(\frac{\tau_w}{\rho a}\right) \tag{2}$$

and for the wall temperature jump condition ,

$$T_{gas} - T_w = \left(\frac{2}{\alpha}-1\right)\frac{2\gamma}{(\gamma+1)P_r} l \left(\ \frac{dT}{dy}_{\ w}\ \right) \tag{3}$$

$f = 1$, τ_w the wall shear stress, a the speed of sound, T_{gas} and T_w are the translational temperature of the gas and the wall temperature, respectively, $\alpha = 1$, γ the ratio of specific heats, and Pr the Prandtl number.

IV. Results

A. Spherical-Nosed Cylinder

Figure 5 illustrate the typical simulated flow field around the nose region of the spherical-nosed cylinder for case 1 in Table 1. The standoff distance of a hypersonic diatomic gas flow over a sphere has been derived in Wen's work [6]. The empirical formula of the stand-off distance of a monatomic-gas supersonic flow is also published in Oliver's work [7] and widely applied in related studies. The stand-off distance of present results can be compared with the equation obtained from the empirical frozen-flow data, which can be written as

$$\frac{\triangle}{D} \ = \ \frac{0.41\rho_\infty}{\rho_s} \tag{4}$$

where D stands for the diameter of the hemisphere, $\triangle$ the standoff distance, ρ_s the density on the stagnation streamline and just behind the shock, and ρ_∞ the free stream density. Table 6 shows the comparison

between the current simulated stand-off distances and the empirical ones (Eq.(4)) for all Argon cases in Table 1

From the results obtained, it is seen that the in-house UNIC-UNS code is capable of providing good predictions of the shock positions for hypersonic flows over spherical-nosed cylinder. The typical comparisons of the pressure coefficients (Cp), skin friction coefficients (Cf) and Stanton numbers (Ch), between our NS simulations with the slip boundary conditions (Case 5, Table 1) and the published DSMC results [3] are shown in Fig. 6.

The definitions of pressure coefficient, skin friction coefficient and Stanton number are as follow:

$$C_p \equiv \frac{p - p_\infty}{\frac{1}{2}\rho_\infty V_\infty^2} \tag{5}$$

$$C_f \equiv \frac{\tau_w}{\frac{1}{2}\rho_\infty V_\infty^2} \tag{6}$$

$$C_h \equiv \frac{q}{\frac{1}{2}\rho_\infty V_\infty^3} \tag{7}$$

where p is the pressure at the point at which pressure coefficient is being evaluated, p_∞ is the freestream pressure, ρ_∞ is the freestream fluid density and q is the convection heat transfer coefficient. In Fig. 6, it can be seen that, despite a relative large discrepancy found in the skin friction comparison, the overall agreement between NS and DSMC simulations are good for the pressure, skin friction and heat transfer distributions.

B. EXPERT

A validation case for the in-house NS solver, for the EXPERT geometry with an roll angle of 45^o and an AoA of -20^o was performed and compared with DSMC[8] computations. As shown in Table 7, good agreement is found. The in-house UNIC-UNS code is validated again.

In the following discussion, the flow analyses of the EXPERT along the decent trajectory through the atmosphere will be presented. Figure 7 shows typical contour distributions including pressure, temperature and Mach number, for the EXPERT capsule, with no roll angle and an AoA of -5.5°at an altitude of 90 km (Air is the test gas). The capsule reaches Mach 18 with a stagnation temperature of 4241.28 K and stagnation Pressure of 85.045 Pa. The stand-off distance is found to be 23.69 mm.

Figure 8 depicts the distributions of pressure, skin friction and heat transfer rate over the EXPERT capsule surface at the altitude of 90 km, with no roll angle and an AoA of -5.5°. Figure 9 shows the Cp, Cf and Ch distributions along the lower centerline of the capsule at different altitudes, with the same flight attitude of Fig. 8. As seen, Cp, Cf and Ch distributions at the altitudes of 90, 80 and 60 km are similar in the trend but different in magnitude.

The Cp, Cf and Ch distributions have their corresponding maximum values located very close to the nose tip. Cp, Cf and Ch decrease monotonically from their maximum-value point toward the flap. The oblique shock generated by the deflected flap (see Fig. 7) causes the abrupt increases of Cp, Cf and Ch over the flap surface, wheres the expansion fans emitted at the rear edge of the flap yield their sudden decreases. Another abrupt decreases of Cp, Cf and Ch at x= 400 mm are causes by the expansion fans emitted at the ellipse-cone junction recess (see Fig. 2). Notably, Cp, Cf and Ch distributions have higher values at higher altitudes. The pressure, skin friction and heat flux actually increase as the EXPERT capsule descends. The increases of the freestream density and velocity from the altitude of 90 km to 60 km result in the higher Cp, Cf and Ch at higher altitudes.

Chemical reactions are extremely important for the rarefied gas dynamics at hypersonic flows, common in reentry conditions. Figure 10 presents the mass fraction distributions of different species at the altitude of 90 km. It is observed that the high amount dissociation and reactions are found in the front face of the EXPERT spacecraft due to the abrupt increase of temperature behind the nearly normal shock around the stagnation region. Notably, only the mass fractions of O2, O, N2 and NO species are significant. The ionization effects are negligible at this flight condition. Figure 11 shows the mass fraction distributions of N2, O2, NO, N and O along the stagnation streamline. It is clearly seen that the amounts of NO, N and O increase behind the shock due to mainly the dissociation and exchange reactions induced by the high temperature inside the shock layer.

V. Conclusion

The all-speed continuum code UNIC-UNS with finite-rate chemistry and slip boundary conditons has been implemented to simulated hypersonic flows in the transition regime over spherical-coned and EXPERT models. The UNIC-UNS code was validated using the kinetic DSMC approach. The skin friction coefficient, Stanton number and pressure distributions over the spherical-cone model in the transition regime show good agreement with the DSMC data. The aerothermodynamic characteristics of the EXPERT capsule for the descent trajectory from 90 to 60km were then studied. Cp, Cf and Ch distributions along the lower centerline of the capsule at the altitudes of 90, 80 and 60 km show the similar trend. The Cp, Cf and Ch distributions reach their corresponding maximum values close to the nose tip, following monotonic decreases toward the flap. The oblique shock generated by the deflected flap causes an abrupt increases of Cp, Cf and Ch over the flap surface, where the expansion fans emitted at the rear edge of the flap yield their sudden decreases. The expansion fans emitted at the ellipse-cone junction recess cause another abrupt decreases of Cp, Cf and Ch. High amount dissociation and reactions are found in the front face of the EXPERT spacecraft due to the abrupt increase of temperature behind the bow shock. Further analyses on the entire descent trajectory of the EXPERT capsule will be conducted in the future for the complete comparison with the flight data once the EXPERT capsule is launched.

Acknowledgments

The authors would like to thank the National Science Council of the Republic of China, Taiwan, for financially supporting this research under Contract No. NSC 100-2923-E-006 -002 -MY3. The authors are also grateful to the National Center for High Performance Computing, Taiwan, for providing the computational resources.

References

[1]Ratti et al, EXPERT - The ESA experimental re-entry test-bed: System overview, 16th AIAA/DLR/DGLR International Space Planes and Hypersonic Systems and Technologies Conference, Bremen, Germany, Oct. 19-22, 2009

[2]Chen, Y.S., Lian, Y.Y., Wu, Bill, and Wu, J.S., Scramjet Combustor Computational Modeling, AIAA Paper 2009-5386 (2009).

[3]Ivanov, M., Kashkovsky, A., Gimelshein, S., Markelov, G., Alexeenko, A., Bondar, Y., Zhukova, G., Nikiforov, S., Vashenkov, P., "SMILE system for 2D/3D DSMC computations," Proceedings of 25th International Symposium on Rarefied Gas Dynamics, St. Petersburg, Russia, 2006, pp. 21-28.

[4]12 Park, C., Assessment of two-temperature kinetic model for ionizing air, Journal of Thermophysics and Heat Transfer, Vol.3, pp.233-244.

[5]White, Frank, Viscous Fluid Flow , Third Edition, McGraw-Hill Mechanical Engineering.

[6]Wen, C. Y. and Hornung, H. G., Non-Equilibrium Dissociating Flow over Spheres, Journal of Fluid Mechanics, Vol. 299, pp. 389-405, 1995.

[7]H. Olivier, A Theoretical Model for the Shock Stand-off Distance in Frozen and Equilibrium Flows, J. Fluid Mech., vol. 413, pp. 345-353, 2000

[8]Pavel Vashchenkov, Alexandr Kashkovsky, Mikhail Ivanov, Numerical Analysis of High-Altitude Aerodynamics of the EXPERT Capsule, West-East High Speed Flow Field Conference 19-22, November 2007 Moscow, Russia

[9]Ye.A. Bondar, A.A. Shershnev, A.N. Kudryavtsev, D.V. Khotyanovsky, S. Yonemura, and M.S. Ivanov, Numerical Study of Hypersonic Rarefied Flows about Leading Edges of Small Bluntness

[10]Wang, T.S., Chen, Y.S., Unified Navier-Stokes Flow field and Performance Analysis of Liquid Rocket Engines, J. Propulsion and Power, Vol. 9, No. 5, pp. 678-685, 1993.

[11]Chen, Y. S., UNIC-UNS Users Manual, Engineering Sciences Incorporated, 2006.

Appendix

Table 1. Test cases for the spherical-nosed cylinder.

Case	Test Gas	Kn	Ref. Length (m)	Ma	p (Pa)	ρ $\left(\frac{kg}{m^3}\right)$	T (K)
1	Ideal Gas (Ar)	0.06	0.01	5	5.29	1.142E-4	219.585
2	Ideal Gas (Ar)	0.06	0.01	10	5.29	1.142E-4	219.585
3	Ideal Gas (Ar)	0.5	0.0023	5	5.29	1.142E-4	219.585
4	Ideal Gas (Ar)	0.5	0.0023	10	5.29	1.142E-4	219.585
5	Non reacting N_2	0.06	0.01	20	5.29	8.754E-5	219.585
6	Non reacting N_2	0.5	0.0023	20	5.29	8.754E-5	219.585

Table 2. Gas parameters of Argon.

Gas Chemistry	Frozen Chemistry
Gas Constant (J/kg K)	208.00
Prandtl Number	0.68
Gamma	1.667

Table 3. Gas parameters of Nitrogen.

Gas Chemistry	Frozen Chemistry
Gas Constant (J/kg K)	287.04
Prandtl Number	0.713
Gamma	1.4

Table 4. Test cases for the EXPERT simulations.

Case	Altitude (km)	Ref. Length (m)	Knudsen Number	Mach Number	Pressure (Pa)	Density $\left(\frac{kg}{m^3}\right)$	Temperature (K)
1	60	0.6	0.00043	15.86	21.959	3.0968E-4	247.02
2	80	0.6	0.00733	17.69	1.0525	1.8458E-5	198.63
3	90	0.6	0.04	18.30	0.1824	3.2400E-6	187.00

Table 5. Park's [5] Reaction rate parameters.

Reaction	T_x	M	C	n	E/k
$O_2 + M \rightarrow O + O + M$	$\sqrt{TT_v}$	N	2.90^{23}	-2.0	59,750
		O	2.90^{23}	-2.0	59,750
		N_2	9.68^{22}	-2.0	59,750
		O_2	9.68^{22}	-2.0	59,750
		NO	9.68^{22}	-2.0	59,750
		e^-	9.68^{22}	-2.0	59,750
$N_2 + M \rightarrow N + N + M$	$\sqrt{TT_v}$	N	1.60^{22}	-1.6	113,200
		O	4.98^{22}	-1.6	113,200
		N_2	3.70^{21}	-1.6	113,200
		O_2	3.70^{21}	-1.6	113,200
		NO	4.98^{21}	-1.6	113,200
		e^-	8.30^{24}	-1.6	113,200
$NO + M \rightarrow N + O + M$	$\sqrt{TT_v}$	N	7.95^{23}	-2.0	59,750
		O	7.95^{23}	-2.0	75,500
		N_2	7.95^{22}	-2.0	75,500
		O_2	7.95^{22}	-2.0	75,500
		NO	7.95^{22}	-2.0	75,500
		e^-	7.95^{22}	-2.0	75,500
$NO + O \rightarrow N + O_2$	T		8.37^{12}	0	19,450
$O + N_2 \rightarrow N + NO$	T		6.44^{17}	-1.0	38,370
$O - O_2^+ \rightarrow O_2 + O^+$	T		6.85^{13}	-0.52	18,600
$N_2 + N^+ \rightarrow N + N_2^+$	T		9.85^{12}	-0.18	12,100
$O + NO^+ \rightarrow NO + O^+$	T		2.75^{13}	0.01	51,000
$N_2 + O^+ \rightarrow O + N_2^+$	T		6.33^{13}	-0.21	22,200
$O_2 + NO^+ \rightarrow NO + O_2^+$	T		1.03^{16}	-0.17	32,400
$NO^+ + N \rightarrow N_2^+ + O$	T		1.70^{13}	0.40	35,500
$O + N \rightarrow NO^+ + e^-$	T		1.53^{09}	0.37	3,200
$O + O \rightarrow O_2^+ + e^-$	T		3.85^{09}	0.49	80,600
$N + N \rightarrow N_2^+ + e^-$	T		1.79^{09}	0.77	67,500
$O + e^- \rightarrow O^+ + 2\ e^-$	T_v	e^-	3.90^{33}	-3.90	158,500
$N + e^- \rightarrow N^+ + 2\ e^-$	T_v	e^-	2.50^{34}	-3.82	168,600

Table 6. Stand-off distance comparison

Case	$\triangle$ Simulation (m)	$\triangle$ Eq. (4) (m)	Diference (%)
1	0.0021500	0.0021198	2.24
2	0.0020000	0.0020310	1.57
3	0.0003087	0.0003034	1.73
4	0.0002845	0.0002918	2.59

Table 7. Comparison between NS and DSMC simulations for the EXPERT capsule.

Parameter	NS	DSMC
Speed (m/s)	5101	5101
Density $\frac{kg}{m^3}$	3.24E-6	3.24E-6
Gas	N_2	N_2
Ch (stag. point)	0. 4764	0.480

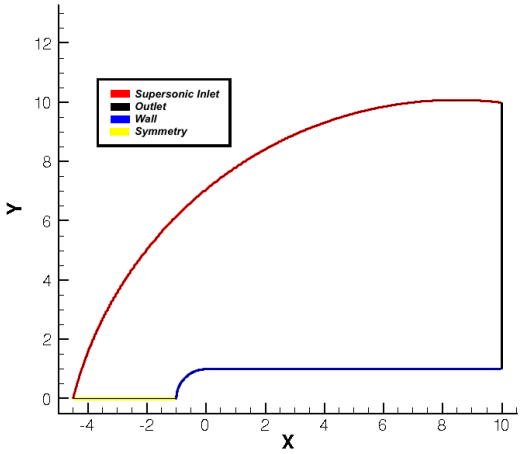

Figure 1. Computational domain and boundary conditions applied to the spherical-nosed cylinder. Used to validate the results from DSMC and NS codes.

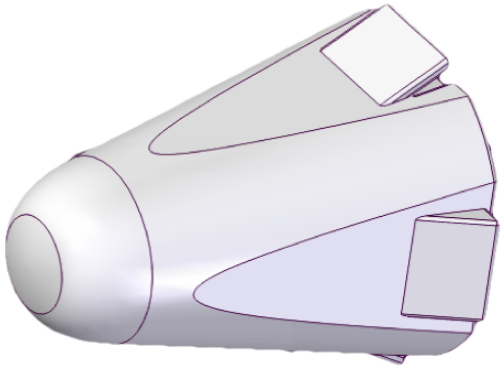

Figure 2. Geometry of the EXPERT capsule.

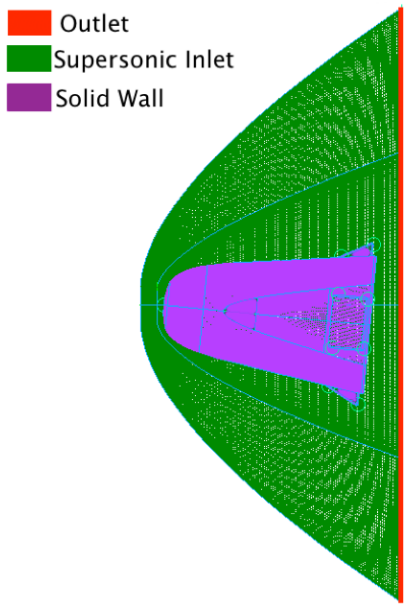

Figure 3. Boundary conditions and Computational domain applied to EXPERT simulations.

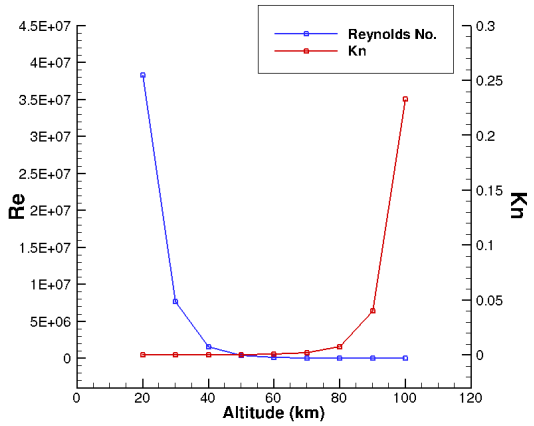

Figure 4. Reynolds numbers and Knudsen numbers vs. altitude

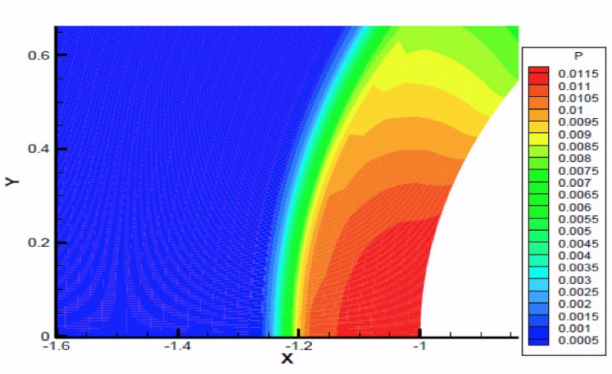

Figure 5. Simulated flow field around the nose region for case 1 in Table 1.

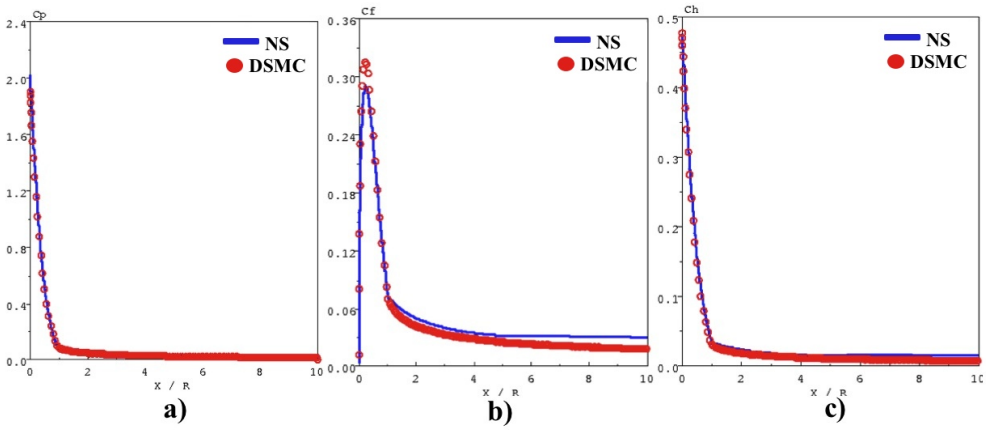

Figure 6. Comparison of (a) Pressure coeffients, (b) skin friction coefficients and (c) Stanton numbers around the spherical-nosed cylinder at Kn=0.06 and Ma=20 between NS and DSMC simulations.

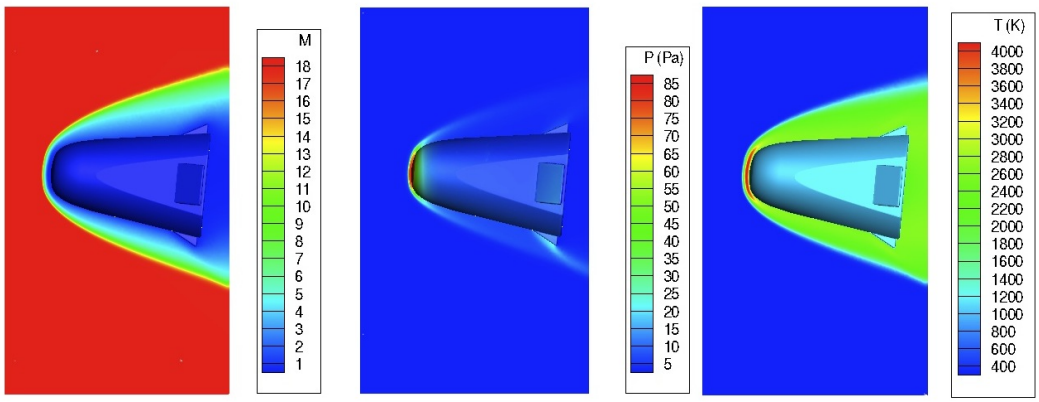

Figure 7. Simulated Mach number, pressure and temperature distributions around the EXPERT capsule at 90km,with no roll angle and an AoA of ?5.5°

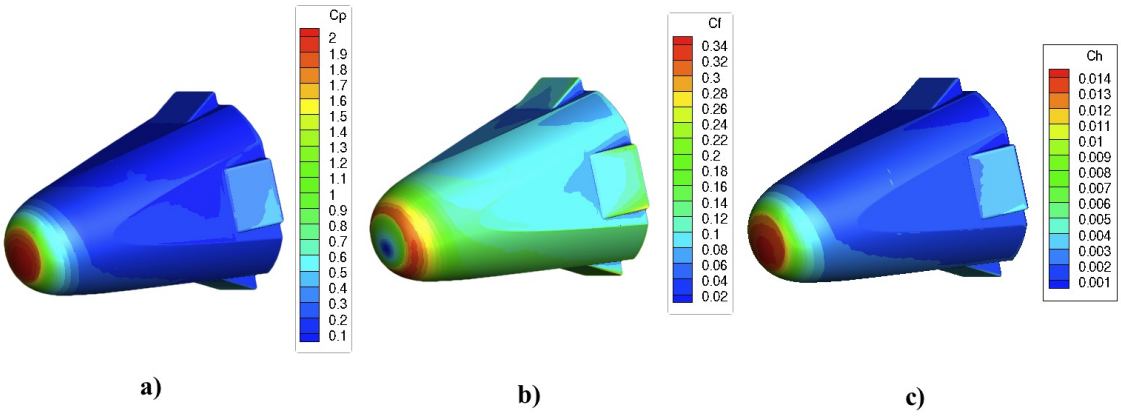

Figure 8. (a) Cp, (b) Cf and (c) Ch distributions over the EXPERT capsule at the altitude of 90km, with no roll angle and an AoA of -5.5°

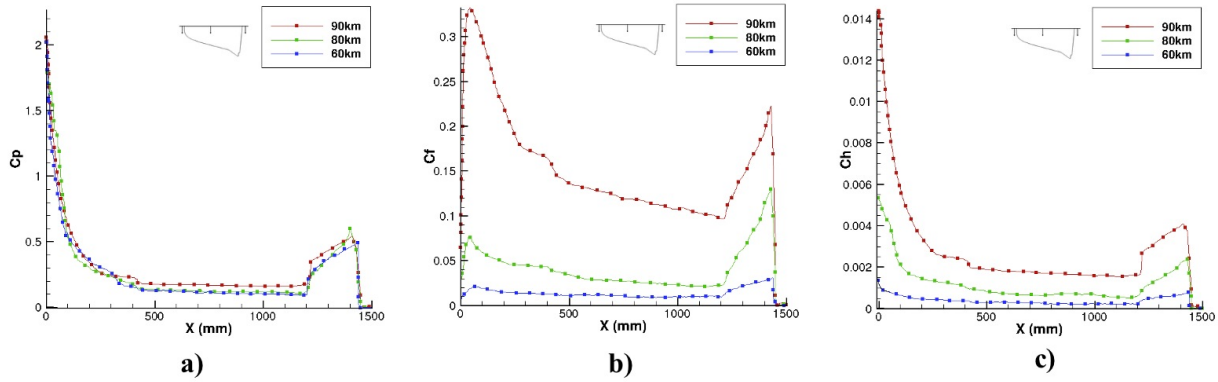

Figure 9. Comparison of Cp(a), Cf (b) and Ch (c) parameters of the EXPERT capsule for different altitudes.

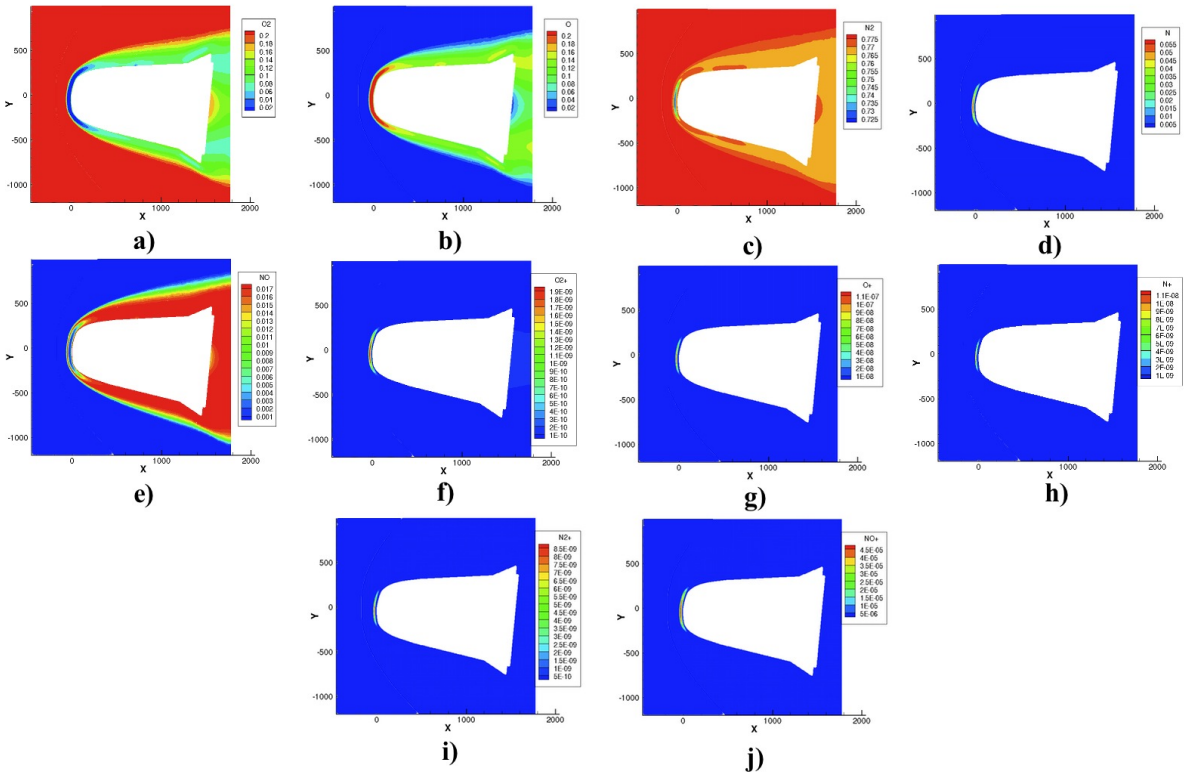

Figure 10. Mass fraction contours of the EXPERT capsule flow for an altitude of 90km. (a) O2; (b) O; (c) N2; (d) N; (e) NO; (f)O2+; (g)O+; (h)N+; (i)N2+; (j)NO+.

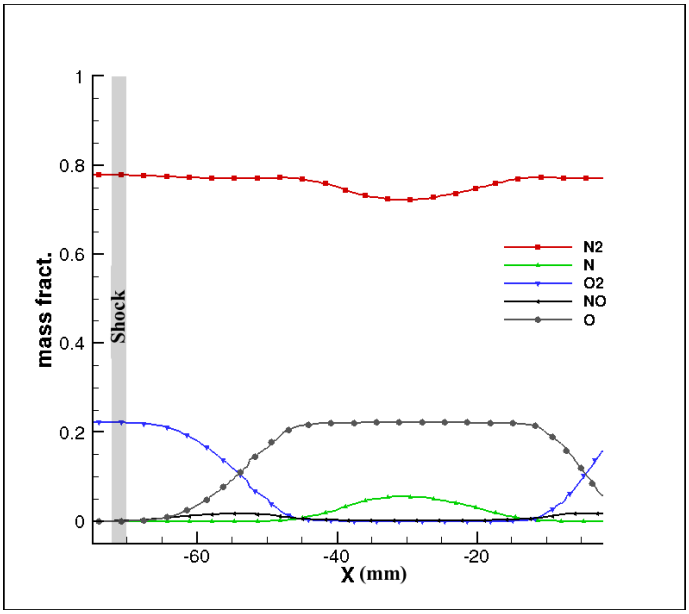

Figure 11. Mass fraction distributions along the stagnation streamline at an altitude of 90km.